AIP | Applied Physics Letters

Elastic constants of cubic and wurtzite boron nitrides

A. Nagakubo, H. Ogi, H. Sumiya, K. Kusakabe, and M. Hirao

Citation: Appl. Phys. Lett. **102**, 241909 (2013); doi: 10.1063/1.4811789
View online: http://dx.doi.org/10.1063/1.4811789
View Table of Contents: http://apl.aip.org/resource/1/APPLAB/v102/i24
Published by the American Institute of Physics.

Elastic constants of cubic and wurtzite boron nitrides

A. Nagakubo,[1] H. Ogi,[1,a)] H. Sumiya,[2] K. Kusakabe,[1] and M. Hirao[1]
[1]*Graduate School of Engineering Science, Osaka University, Toyonaka, Osaka 560-8531, Japan*
[2]*Advanced Materials R & D Laboratories, Sumitomo Electric Industries, Ltd., Itami, Hyogo 664-0016, Japan*

(Received 19 May 2013; accepted 3 June 2013; published online 20 June 2013)

We synthesized pure polycrystalline cubic boron nitride (cBN) and wurtzite boron nitride (wBN) by the direct conversion method from hexagonal boron nitride, and measured their longitudinal-wave elastic constants C_L between 20 and 300 K using picosecond ultrasound spectroscopy. Their room-temperature values are 945 ± 3 GPa and 930 ± 18 GPa for cBN and wBN, respectively. The shear modulus G of cBN was also determined by combining resonance ultrasound spectroscopy and micromechanics calculation as $G = 410$ GPa. We performed *ab-initio* calculations and confirmed that the generalized gradient approximation potential fails to yield correct elastic constants, which indicated the necessity of a hybrid-functional method. © *2013 AIP Publishing LLC*.
[http://dx.doi.org/10.1063/1.4811789]

Cubic boron nitride (cBN) and wurtzite boron nitride (wBN) are expected to exhibit many superior properties, such as high hardness, high elastic stiffness, low thermal expansivity, high thermal conductivity, and so on.[1–5] However, their elastic stiffness remains unclear because of the difficulty of synthesizing high-purity specimens. Because only small specimens were previously available and their sound velocities were very large, conventional ultrasonic methods for stiffness were inapplicable. Many studies, therefore, predicted their elastic constants by theoretical calculations. However, the calculation result depends highly on the interatomic potential and the calculation parameters [as will be shown], and previous values disagree significantly with each other; their standard deviation exceeds 25% for the bulk modulus of cBN, for example, and some calculations even indicate higher bulk modulus of cBN than that of cubic diamond.[6–8] Thus, it is very important to accurately measure the elastic stiffness of BNs to guide theory.

Recently, pure nano-polycrystalline diamonds were synthesized by the direct-conversion method from graphite, which showed hardness higher than that of a monocrystal diamond.[9,10] Here, a similar synthesizing technique was applied for cBNs and wBNs using the starting material of hexagonal boron nitride (hBN), which yields millimeter-order-size specimens.

There are a few previous reports on the elastic constants of cBN. They used Brillouin-scattering[11,12] or x-ray-diffraction (XRD)[13,14] methods. The XRD method estimates the bulk modulus and is inefficient for high-stiffness material because of small strains. There is only one report on measurements of the elastic constants of wBN using the pulse-echo method,[15] where the elastic constants of wBN were estimated to be much smaller than that of cBN (the longitudinal-wave elastic constant C_L of cBN and wBN were 908 GPa and 641 GPa, respectively). However, because the highest purity of wBN was 80% in that study, we consider that the resultant values fail to represent those of wBN.

In this study, we measured C_L of polycrystalline cBN and wBN between 20 and 300 K using picosecond ultrasound spectroscopy (PUS).[16–18] This method uses a femto-second pump light pulse to excite high-frequency coherent phonons and a probe light pulse to detect its sound velocity. High frequency (~200 GHz) and short wavelength (~100 nm) ultrasound allows us to determine the elastic constant accurately even for a small specimen. Concerning cBN, we also determined the shear modulus G using resonance ultrasound spectroscopy (RUS) and micromechanics calculation.

Finally, we performed *ab-initio* calculations using the plane-wave self-consistent field code of QUANTUM ESPRESSO (QE) package[19] and the Vienna *ab-initio* simulation package (VASP).[20]

Our cBN and wBN specimens were synthesized by the direct conversion from hBN under high pressure at high temperature. A high-purity powdered hBN containing impurity of B_2O_3 less than 0.03 wt. % was used as the starting material. Detail conditions for cBN (about 8 GPa and 2300 °C) appear elsewhere[21,22] and we applied relatively high pressure (~20 GPa) and low temperature (~1300 °C) for wBN.[23] Figure 1 shows representative XRD spectra for our BN specimens, which yielded the lattice parameters (a and c) and mass density ρ as follows: $a = 3.6169 \pm 0.0005$ Å and $\rho = 3484.7 \pm 0.5\ \mathrm{kg/m^3}$ for cBN, and $a = 2.5494 \pm 0.0015$ and $c = 4.2229 \pm 0.0004$ Å, and $\rho = 3467.4 \pm 4.3\ \mathrm{kg/m^3}$ for wBN.

As shown in Fig. 1(a), the XRD measurement for our cBN specimens detected diffraction peaks caused only by the cBN structure, including no peaks related to other phases. The spectrum clearly shows peaks caused by Kα1 and Kα2 rays at higher diffraction angle. Therefore, our cBNs show high purity and crystallinity. Concerning our wBNs, we also detected diffraction peaks from the wBN-crystal planes, while a small (0002) peak from the residual hBN phase was detected. However, its height was only ~2% of the maximum peak of wBN. Note that the previous reports for cBN did not show an XRD spectrum.[24,25] Some reports showed the XRD spectrum, but it showed many impurities.[26,27] A recent hypothermal method succeeded in obtaining cBN as pure as our specimens, but wBN phase is still included.[28] No previous studies showed such an XRD spectrum in Fig. 1(b) for wBN showing nearly only wBN peaks[29,30] except powder

a)ogi@me.es.osaka-u.ac.jp

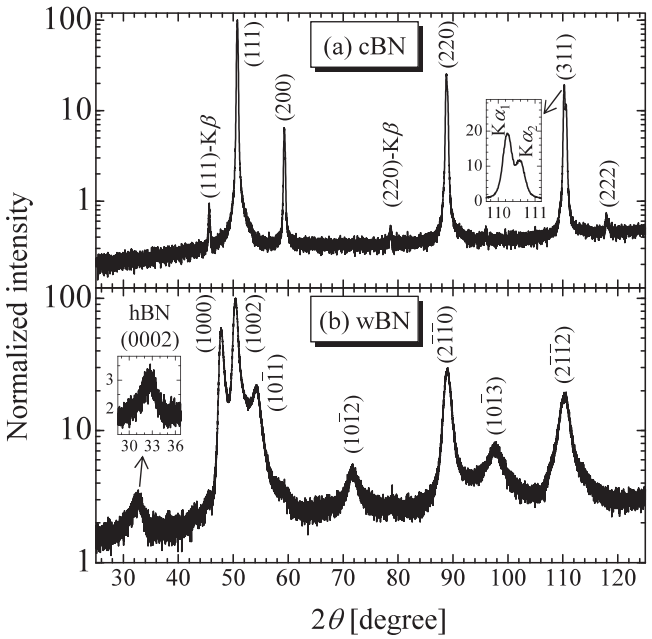

FIG. 1. XRD spectra of (a) cBN and (b) wBN.

specimens,[31] and we consider that we have succeeded in synthesizing highly pure bulk wBN. cBNs have fine-grained (100–500 nm) structure, and wBNs show lamellar structure as well as granular structure; their domain size varies between 50 and 1000 nm. These XRD measurements indicated that crystallographic axes in our specimens are oriented disorderly, showing no textures, and they are macroscopically isotropic materials.

The optics we developed for picosecond ultrasound spectroscopy at low temperatures is shown in our previous research.[32,33] We used a cryostat as a specimen holder and applied the light pulses to the specimen through a glass window. The specimen was attached on a Cu heat exchanger cooled by liquid He, and we used a semiconductor thermometer attached to the heat exchanger to measure the specimen temperature. We deposited a 10 nm Pt thin film on each specimen surface, which absorbs the pump light energy for excitation of ultrasound. The time-delayed probe light pulse is reflected at the surface, but a part of the probe light is transmitted inside the specimen. The transmitted probe light is diffracted backward via the piezo-optic effect, which causes interference with the surface-reflected light, resulting in an oscillating signal in the reflected probe light as the ultrasound propagates. This oscillation signal is called the Brillouin oscillation, and its frequency f relates to the sound velocity via Bragg's condition

$$f = \frac{2nv}{\lambda}, \tag{1}$$

where λ is the wavelength of the probe light, v is the sound velocity, and n is the refractive index. We measured n by ellipsometry[34] using instrument M-2000 produced by J. A. Woollam Co. The ellipsometric angles were measured as a function of the wavelength between 370 and 1000 nm, and the Cauchy model was used to determine inversely the refractive index. From reproducibility and the fitting residual error, we estimate the possible error in the measured refractive index to be less than 1%. We can then determine C_L by measuring the Brillouin-oscillation frequency f through $C_L = \rho f^2 \lambda^2/(4n^2)$. The penetration depth of the observed ultrasound is about 2 μm, and the laser diameter is 50 μm. This measurement volume includes a sufficiently large number of grains, and the resultant elastic constant corresponds to the quasi-isotropic polycrystalline value.

Figure 2 shows typical Brillouin oscillations and corresponding Fourier spectra measured in cBN and wBN. We measured the Brillouin oscillation signals at about ten different points on each specimen, and determined the elastic constant with the error bar. Figure 3 shows temperature dependence of C_L of cBN, wBN, and diamond.[35] [The error bars are shown for BNs' elastic constants.] Low temperature elastic constants are important since they are related to Debye temperature, Grüneisen parameter, and other physical properties.[36,37] More importantly, most *ab-initio* calculations neglect phonon vibrations, corresponding to the ground state at 0 K. Therefore, cryogenic measurements are necessary for comparisons between experimental and calculation results. We found that BNs are nearly temperature independent [like diamond], and the elastic constant at cryogenic temperatures is the same as at room temperature within the error bar. The room-temperature values of C_L of cBN and wBN are 945 ± 3 GPa and 930 ± 18 GPa, respectively.

We succeeded in fabricating a larger rectangular parallelepiped specimen of cBN, and determined its macroscopic elastic constants by the RUS method with needle-tripod transducers.[38] [Concerning wBN, we cannot synthesize a large enough specimen for RUS.] The RUS method determines all the independent elastic constants inversely by measuring many free-vibration resonance frequencies.[39,40] The needle-tripod transducers enable us to measure ideal free-vibration frequencies because no biasing external force is applied to the specimen except for gravity.[38] Using this

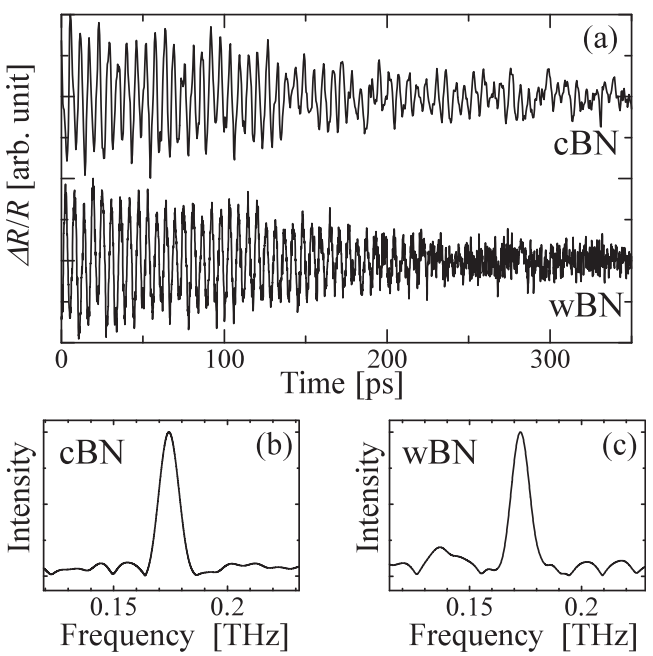

FIG. 2. (a) Observed Brillouin oscillations of cBN and wBN and corresponding Fourier spectra of (b) cBN and (c) wBN. Strong coherent oscillations can be observed.

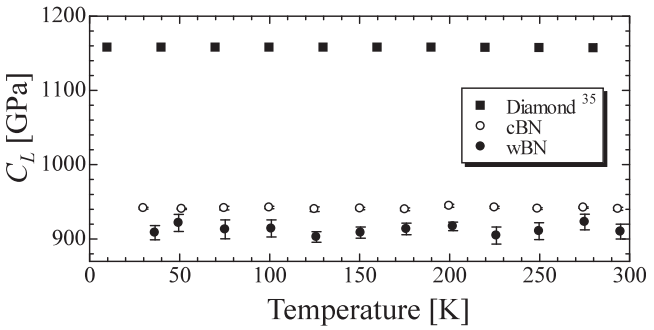

FIG. 3. Temperature behaviors of C_L for cBN (open circle), wBN (closed circle), and diamond (closed square, see Ref. 35). They are nearly temperature independent. Error bars of cBN are smaller than their symbols.

method, we determined two isotropic elastic constants, C_L and the shear modulus G. The specimen measured $2.6365 \times 2.5445 \times 1.1705$ mm^3, and we obtained its mass density $\rho = 3416\,\text{kg/m}^3$ from the volume and its mass. This value is smaller than the XRD mass density by 2%, indicating presence of a few defects inside the material. Because temperature and pressure near the center of the specimen would not be as high as near the surface, unbounded region and defects might be included between grains. Because picosecond ultrasonic spectroscopy measures elasticity near the surface where temperature and pressure equal the intended values, these defects will be absent and ideal values will be obtained.

C_L and G of cBN measured by RUS are 899 GPa and 391 GPa, respectively, and so the RUS C_L is smaller than that measured by picosecond ultrasound spectroscopy by 5%. We attribute this underestimation of C_L to the defects in the RUS specimen because the apparent mass density is smaller than the XRD mass density by 2%. To estimate the effect of defects, we consider the C_L measured by picosecond ultrasound spectroscopy as the true value, and calculate underestimated elastic constants of the RUS specimen through a micromechanics calculation.[41] First, we consider the RUS specimen as a composite consisting of cBN matrix and spherical cavities for the defects. The composite elastic constants can be calculated by Eshelby's equivalent inclusion theory using Mori-Tanaka mean-field modeling[42,43] through following equations:

$$\mathbf{C}_C = \mathbf{C}_M + V_f(\mathbf{C}_I - \mathbf{C}_M)\mathbf{A}, \tag{2}$$

$$\mathbf{A} = \mathbf{A}_D[(1 - V_f)\mathbf{I} + V_f\mathbf{A}_D]^{-1}, \tag{3}$$

$$\mathbf{A}_D = [\mathbf{I} + \mathbf{S}\mathbf{C}_M^{-1}(\mathbf{C}_I - \mathbf{C}_M)]^{-1}. \tag{4}$$

Here, $\mathbf{C}_C$, $\mathbf{C}_M$, and $\mathbf{C}_I$ denote the elastic stiffness tensors of the composite, the matrix, and the inclusions, respectively, V_f denotes the volume fraction, and $\mathbf{S}$ the Eshelby tensor. Because one of the matrix elastic constants, C_L, and two composite elastic constants, $\mathbf{C}_C$, are known, we can inversely determine the matrix shear modulus G and the porosity by fitting the predicted composite elastic constants to the RUS measurements. Using the least-squares fitting method, we determined them; $G = 410$ GPa and the $V_f = 2.28\%$. Thus, the determined porosity approximates the measurement, confirming the inversely determined shear modulus of cBN.

Among previous measurements, the latest reported values on cBN using Brillouin scattering (BS)[12] provided C_L and G lower than our values by 3%. We attributed this discrepancy to two factors. First, the picosecond ultrasound spectroscopy is more accurate: It can excite coherent phonons, which directly interact with the probe light to cause a strong backscattering signal, whereas the Brillouin-scattering method needs to use weak spontaneous phonons. Therefore, the signal-to-noise ratio is usually higher in picosecond ultrasound spectroscopy. Besides, the apparent quality factor (Q value) is larger in picosecond ultrasound spectroscopy than in Brillouin scattering. The former can observe direct interaction between the excited high-frequency phonon and the probe light during the propagation of the phonon pulse. On the other hand, it is very difficult to adopt the backscattering setup in the latter because the reflected light is so strong, and usually an angled setup is used. In this case, however, the interacting region is restricted and the apparent Q value decreases. In fact, for BNs, the Q values of previous reports using Brillouin scattering were also about 10, but our Q value is about 20. This difference is important because the previous studies used monocrystal specimens, whereas we used polycrystalline specimens, whose Q values decrease because of grain scattering. Second, our specimen shows

TABLE I. Measured (PUS, BS, XRD), calculated, and reported lattice parameter [Å] and elastic constants [GPa] of cBN. We averaged the equivalent calculational method for GGA, LDA, hybrid functional method, and molecular dynamics (MD), respectively. Error means the standard deviation among the previously reported values.

		a	C_L	G	B
This work	PUS	3.6169 ± 0.0005	945 ± 3	410[a]	401[a]
	QE-GGA	3.622	887	384	375
	VASP-GGA	3.626	881	381	372
	QE-LDA	3.569	951	412	402
	VASP-LDA	3.583	940	403	402
Reference (measured)	BS[b]		941	405	400
	BS[c]	3.6157 ± 0.0008	913	399	381
	XRD[d]	3.615 ± 0.002			369 ± 14
	XRD[e]	3.6157 ± 0.0008			387 ± 4
Reference (calculated)	GGA[f]	3.620±0.007[g]	920±38[g]	390±21[g]	385±16[g]
	LDA[h]	3.589±0.012[g]	946±15[g]	408±9[g]	398±12[g]
	hybrid[i]	3.602±0.006[g]			399±7[g]
	MD[j]	3.625±0.023[g]	858±58[g]	360±43[g]	378±2[g]
	Force field[k]		1074	342	618
	Tight binding[l]		1079	341	624
	Tight binding[m]		1310	430	737

[a]Determined by the RUS method and micromechanics calculation.
[b]Reference 11.
[c]Reference 12.
[d]Reference 13.
[e]Reference 14.
[f]References 49–52.
[g]Average and standard deviation of previously reported calculation results.
[h]References 49, 51, 53–59.
[i]References 60–62.
[j]References 63–65.
[k]Reference 6.
[l]Reference 7.
[m]Reference 8.

TABLE II. Measured (PUS), calculated, and reported lattice parameters [Å] and elastic constants [GPa] of wBN. We averaged the reported calculational results. Error means the standard deviation among the previously reported values.

		a	*c*	C_L	*G*	*B*
This work	PUS	2.5494 ± 0.0015	4.2229 ± 0.0004	930 ± 18		
	QE-GGA	2.553	4.223	885	384	373
	VASP-GGA	2.556	4.226	882	383	372
	QE-LDA	2.515	4.162	950	412	401
	VASP-LDA	2.525	4.178	940	404	402
Reference(calculated)	LDA[a]	2.538±0.005[b]	4.185±0.011[b]	937±17[b]	407±11[b]	394±4[b]

[a]References 54, 57, 59, 66, and 67.
[b]Average and standard deviation of previously reported calculation results.

higher purity. The previous studies[11,12] did not show any proofs for structural purity, such as an XRD spectrum.

Finally, we calculated the lattice parameters and elastic constants of cBN and wBN using QE and VASP based on density functional theory (DFT). QE uses a plane-wave pseudopotential method and VASP uses projector augmented wave (PAW) method. We adopted the local-density-approximation (LDA) and generalized gradient approximation (GGA) as the exchange correlation potential for each method. The cutoff energy of plane wave and the *k*-point mesh in QE are 2180 eV and $10 \times 10 \times 10$, and these in VASP are 1300 eV and $11 \times 11 \times 11$, respectively. In the QE package, we used Ceperley-Alder exchange correlation for LDA[44] parameterized by Perdew and Zunger[45] and used the Perdew and Wang scheme[46] for GGA. In VASP, we also used the same LDA method, whereas we used the method of Perdew and Burke and Ernzerhof[47] for GGA. We calculated the elastic constants through the relationship between the applied strain (±1%) and the total energy change.[48] At each deformation, we performed the ion-relaxation process. [The ion-relaxation procedure affected little the cBN elastic constants, but it decreased the wBN elastic constants approximately by 10 GPa.] The resultant lattice parameters and elastic constants are given in Tables I and II. There is no noticeable difference in the calculated values between QE using pseudopotential and VASP using PAW. The important result is that calculation with the GGA fails to provide the elastic constants close to the measurements, while it yields the lattice parameters close to the measurements. On the other hand, calculation with the LDA provides better elastic constants, but it gives lattice parameters smaller than measurements. A similar tendency is seen in previous calculations based on our measurement: the GGA leads to proper lattice constants and the LDA leads to proper elastic constants. We show their detail values in the supplemental material.[68] Our measurement results reveal that the tendency is the same for wBN. Recently, to improve DFT calculation, several hybrid functional methods, which represent a sensible compromise between DFT and Hartree-Fock approaches, have been proposed.[60–62] It has been pointed out that calculations with LDA and GGA fail to estimate electronic properties, such as the band gap, and structural properties, such as lattice constants simultaneously.[60] For example, calculated band-gap values of cBN using GGA, LDA, and a hybrid functional method are 4.45, 4.51, and 5.98 eV, respectively, while its experimental value is 6.22 eV.[60] Thus, hybrid functional methods provide better electronic properties.[60–62] More importantly, they succeeded in predicting a bulk modulus close to our measurement as well as a lattice constant for cBN as shown in the supplemental material (Table S1).[68]

In summary, we measured the elastic constants of highly pure cBN and wBN synthesized by high-temperature high-pressure direct conversion method using picosecond ultrasound spectroscopy between 20 and 300 K. It is found that their elastic constants are nearly temperature independent, and their longitudinal-wave moduli are similar. Most traditional local or semilocal DFT calculations fail to estimate the lattice parameters and the elastic constants simultaneously. The hybrid-functional method seems to provide materials properties more accurately, although it merely adjusts parameters for fitting the calculations to measurements. Therefore, improvement in the theoretical calculation will be required, where our measurement results will be needed for evaluating calculation accuracy.

[1]Z. Pan, H. Sun, Y. Zhang, and C. Chen, Phys. Rev. Lett. **102**, 055503 (2009).
[2]G. A. Slack and S. F. Bartram, J. Appl. Phys. **46**, 89 (1975).
[3]P. J. Gielisse, S. S. Mitra, J. N. Plendl, R. D. Griffis, L. C. Mansur, R. Marshall, and E. A. Pascoe, Phys. Rev. **155**, 1039 (1967).
[4]C. W. Chang, A. M. Fennimore, A. Afanasiev, D. Okawa, T. Ikuno, H. Garcia, D. Li, A. Majumdar, and A. Zettl, Phys. Rev. Lett. **97**, 085901 (2006).
[5]E. K. Sichel, R. E. Miller, M. S. Abrahams, and C. J. Buiocchi, Phys. Rev. B **13**, 4607 (1976).
[6]C. M. Marian, M. Gastreich, and J. D. Gale, Phys. Rev. B **62**, 3117 (2000).
[7]M. Ferhat, A. Zaoui, M. Certier, and H. Aourag, Physica B **252**, 229 (1998).
[8]D. N. Talwar, D. Sofranko, C. Mooney, and S. Tallo, Mater. Sci. Eng. B **90**, 269 (2002).
[9]T. Irifune, A. Kurio, S. Sakamoto, T. Inoue, and H. Sumiya, Nature **421**, 599 (2003).
[10]H. Sumiya and T. Irifune, Diamond Relat. Mater. **13**, 1771 (2004).
[11]M. Grimsditch, E. S. Zouboulisa, and A. Polian, J. Appl. Phys. **76**, 832 (1994).
[12]J. S. Zhang, J. D. Bass, T. Taniguchi, A. F. Goncharov, Y. Y. Chang, and S. D. Jacobsen, J. Appl. Phys. **109**, 063521 (2011).
[13]E. Knittle, R. M. Wentzcovitch, R. Jeanloz, and M. L. Cohe, Nature **337**, 349 (1989).
[14]A. F. Goncharov, J. C. Crowhurst, J. K. Dewhurst, S. Sharma, C. Sanloup, E. Gregoryanz, N. Guignot, and M. Mezouar, Phys. Rev. B **75**, 224114 (2007).
[15]A. V. Bochko and O. I. Zaporozhets, Powder Metall. Met. Ceram. **34**, 417 (1995).
[16]A. Devos and R. Cote, Phys. Rev. B **70**, 125208 (2004).
[17]P. Emery and A. Devos, Appl. Phys. Lett. **89**, 191904 (2006).

[18]H. Ogi, T. Shagawa, N. Nakamura, and M. Hirao, Phys. Rev. B **78**, 134204 (2008).
[19]P. Giannozzi, S. Baroni, N. Bonini, M. Calandra, R. Car, C. Cavazzoni, D. Ceresoli, G. L. Chiarotti, M. Cococcioni, I. Dabo *et al.*, J. Phys.: Condens. Matter **21**, 395502 (2009).
[20]G. Kresse and J. Hafner, Phys. Rev. B **47**, 558 (1993).
[21]H. Sumiya, S. Uesaka, and S. Satoh, J. Mater. Sci. **35**, 1181 (2000).
[22]H. Sumiya and S. Uesaka, J. Jpn. Soc. Powder Metall. **49**, 327 (2002).
[23]Y. Ishida and H. Sumiya, in *Proceedings of the 2012 Powder Metallurgy World Congress & Exhibition*, edited by H. Miura and A. Kawasaki, 18D-T13-28 (The Japan Society of Powder and Powder Metallurgy, Yokohama, 2012).
[24]F. P. Bundy and R. H. Wentorf, J. Chem. Phys. **38**, 1144 (1963).
[25]N. L. Coleburn and J. W. Forbes, J. Chem. Phys. **48**, 555 (1968).
[26]T. Sato, H. Hiraoka, T. Endo, O. Fukunaga, and M. Iwatan, J. Mater. Sci. **16**, 1829 (1981).
[27]T. Sato, T. Endo, S. Kashima, O. Fukunaga, and M. Iwata, J. Mater. Sci. Lett. **18**, 3054 (1983).
[28]G. Lian, X. Zhang, L. Zhu, D. Cui, Q. Wang, and X. Tao, J. Solid State Chem. **182**, 1326 (2009).
[29]F. R. Corrigan and F. P. Bundy, J. Chem. Phys. **63**, 3812 (1975).
[30]T. Sato, T. Ishii, and N. Setaka, J. Am. Ceram. Soc. **65**, c162 (1982).
[31]T. Soma, A. Sawaoka, and S. Saito, Mater. Res. Bull. **9**, 755 (1974).
[32]K. Tanigaki, T. Kusumoto, H. Ogi, N. Nakamura, and M. Hirao, Jpn. J. Appl. Phys. Part 1 **49**, 07HB01 (2010).
[33]A. Nagakubo, A. Yamamoto, K. Tanigaki, H. Ogi, N. Nakamura, and M. Hirao, Jpn. J. Appl. Phys. Part 1 **51**, 07GA09 (2012).
[34]H. G. Tompkins and W. A. McGahan, *Spectroscopic Ellipsometry and Reflectometry* (Wiley, New York, 1999).
[35]A. Migliori, H. Ledbetter, R. G. Leisure, C. Pantea, and J. B. Betts, J. Appl. Phys. **104**, 53512 (2008).
[36]V. P. Varshni, Phys. Rev. B **2**, 3952 (1970).
[37]H. Ledbetter, Phys. Status Solidi B **181**, 81 (1994).
[38]H. Ogi, K. Sato, T. Asada, and M. Hirao, J. Acoust. Soc. Am. **112**, 2553 (2002).
[39]I. Ohno, J. Phys. Earth **24**, 355 (1976).
[40]A. Migliori and J. Sarrao, *Resonant Ultrasound Spectroscopy* (Wiley, New York, 1997).
[41]H. Ogi, N. Nakamura, H. Tanei, M. Hirao, R. Ikeda, and M. Takemoto, Appl. Phys. Lett. **86**, 231904 (2005).
[42]T. Mori and K. Tanaka, Acta Metall. **21**, 571 (1973).
[43]T. Mura, *Micromechanics of Defects in Solids*, 2nd ed. (Martinus Nijhoff, Netherlands, 1987).
[44]D. M. Ceperley and B. J. Alder, Phys. Rev. Lett. **45**, 566 (1980).
[45]J. P. Perdew and A. Zunger, Phys. Rev. B **23**, 5048 (1981).
[46]J. P. Perdew and Y. Wang, Phys. Rev. B **45**, 13244 (1992).
[47]J. P. Perdew, K. Burke, and M. Ernzerhof, Phys. Rev. Lett. **77**, 3865 (1996).
[48]L. Fast, J. M. Wills, B. Johansson, and O. Eriksson, Phys. Rev. B **51**, 17431 (1995).
[49]R. Mohammad and S. Katircioglu, J. Alloys Compd. **478**, 531 (2009).
[50]Y. D. Guo, X. D. Yang, X. B. Li, X. S. Song, and X. L. Cheng, Diamond Relat. Mater. **17**, 1 (2008).
[51]S. Saib and N. Bouarissa, J. Alloys Compd. **448**, 11 (2008).
[52]A. Zaoui and F. E. H. Hassan, J. Phys.: Condens. Matter **13**, 253 (2001).
[53]R. M. Wentzcovitch, K. J. Chang, and M. L. Cohen, Phys. Rev. B **34**, 1071 (1986).
[54]K. Kim, W. R. L. Lambrecht, and B. Segall, Phys. Rev. B **53**, 16310 (1996).
[55]Y. J. Hao, X. R. Chen, H. L. Cui, and Y. L. Bai, Physica B **382**, 118 (2006).
[56]M. B. Kanoun, A. E. Merad, G. Merad, J. Cibert, and H. Aourag, Solid-State Electron. **48**, 1601 (2004).
[57]K. Karch and F. Bechstedt, Phys. Rev. B **56**, 7404 (1997).
[58]P. R. Hernandez, M. G. Diaz, and A. Munoz, Phys. Rev. B **51**, 14705 (1995).
[59]K. Shimada, T. Sota, and K. Suzuki, J. Appl. Phys. **84**, 4951 (1998).
[60]J. Heyd, J. E. Peralta, G. E. Scuseria, and R. L. Martin, J. Chem. Phys. **123**, 174101 (2005).
[61]J. Paier, M. Marsman, K. Hummer, G. Kresse, I. C. Gerber, and J. G. Angyan, J. Chem. Phys. **124**, 154709 (2006).
[62]J. Paier, M. Marsman, and G. Kresse, J. Chem. Phys. **127**, 024103 (2007).
[63]W. H. Moon and H. J. Hwang, Mater. Sci. Eng. B **103**, 253 (2003).
[64]W. H. Moon, M. S. Son, and H. J. Hwang, Physica B **336**, 329 (2003).
[65]W. H. Moon and H. J. Hwang, Appl. Surf. Sci. **239**, 376 (2005).
[66]S. Saib and N. Bouarissa, Diamond Relat. Mater. **18**, 1200 (2009).
[67]K. Shimada, Jpn. J. Appl. Phys. Part 2 **45**, L358 (2006).
[68]See supplementary material at http://dx.doi.org/10.1063/1.4811789 for details of previous calculations.